Research Square

Preprints are preliminary reports that have not undergone peer review.
They should not be considered conclusive, used to inform clinical practice,
or referenced by the media as validated information.

Experimental Study and Response Surface Modeling of the Combined Effects of the Process Parameters on the Thermal and Mechanical Properties of Friction Stir Welded 3003 Aluminum Alloy

amina belaribi

belaribiamina5@gmail.com

Universite Djillali Liabes Faculte de Technologie https://orcid.org/0009-0007-4588-7927

Abdelkader Miloudi

University of Djillali Liabes Faculty of Technology: Universite Djillali Liabes Faculte de Technologie

Ben Messaoud Mohammed Abdelghani

University of Djillali Liabes Faculty of Technology: Universite Djillali Liabes Faculte de Technologie

Mohammed Nadhir Djamel Eddine Cherief

University of Djillali Liabes Faculty of Technology: Universite Djillali Liabes Faculte de Technologie

Abdelkader Boulenouar

University of Djillali Liabes Faculty of Technology: Universite Djillali Liabes Faculte de Technologie

Mohammed Bouchelarm

University of Djillali Liabes Faculty of Technology: Universite Djillali Liabes Faculte de Technologie

Research Article

Keywords: FSW, AA3003, feed rate, response surface methodology, hardness

Posted Date: November 17th, 2026

DOI: https://doi.org/10.21203/rs.3.rs-11501119/v1

License: This work is licensed under a Creative Commons Attribution 4.0 International License.
Read Full License

Experimental Study and Response Surface Modeling of the Combined Effects of the Process Parameters on the Thermal and Mechanical Properties of Friction Stir Welded 3003 Aluminum Alloy

Amina Belaribi[1]*, Abdelkader Miloudi[1] , Ismail Chekalil[2], Ben Messaoud Mohammed Abdelghani [1],Mohammed Nadhir Djamel Eddine Cherief[1], Abdelkader Boulenouar[1], Mohammed Bouchelarm[1]

[1]University of Djillali Liabes, Laboratory of Materials and Reactive Systems (LMSR), Sidi Bel Abbès, Algeria

[2]IRC for Intelligent Manufacturing and Robotics, King Fahd University of Petroleum and Minerals. SA

*Corresponding author:
belaribiamina5@gmail.com
Contributing authors:
miloudidz@yahoo.fr;
ismail.chekalil@kfupm.edu.sa;
abdelghanibenmessaoud00@gmail.com;
n.cherief@yahoo.com;
aek_boulenouar@yahoo.fr;
m.bouchelarm@yahoo.com

Abstract

Friction stir welding (FSW) of AA3003 aluminum alloy is governed by the tool rotational speed (N), feed rate (S), and tilt angle (θ). Earlier studies on this alloy have used these parameters to model either the tensile properties or the welding temperature, but these responses have rarely been analyzed together with the hardness of the weld zones. In this study, a three-level full factorial design and response surface methodology (RSM) were used to model four responses: the ultimate tensile strength (σ_U), the maximum temperature (Tmax) recorded 10 mm from the weld centerline, and the hardness of the nugget zone (NZ) and the heat-affected zone (HAZ). Within the tested ranges, the tilt angle had the largest effect on Tmax, whereas the rotational speed had the largest effect on NZ hardness and σ_U. Increasing N or θ raised Tmax and lowered the hardness of both zones, while σ_U increased with N and varied nonlinearly with S, with a minimum near the intermediate feed rate. A multi-response optimization that maximized σ_U and hardness gave N = 1000 rpm, S = 400 mm/min, and θ = 0.5°. At this setting, the predicted σ_U and the NZ and HAZ hardness reached about 77%, 89%, and 80% of the base metal values, respectively. Eight independent validation tests gave coefficients of determination (R^2) between 0.818 and 0.919. The models describe the parameter effects within the tested domain and can support the selection of welding conditions for AA3003 joints.

Keywords: FSW, AA3003, feed rate, response surface methodology, hardness.

1. Introduction

Friction stir welding (FSW) is a solid-state joining process in which a rotating tool heats and stirs the material without melting it. It was invented in 1991 by the TWI (The Welding Institute) in the United Kingdom [1]. This process allows for welds to be made without filler material and without melting the base material, which eliminates solidification phenomena and thus reduces the risk of porosity and hot cracking [2], [3]. Furthermore, no arc is involved and far fewer fumes are produced than in fusion welding, which improves safety and the work environment [4]. FSW can also join alloys that are difficult to weld by fusion processes, and it is now used in several industrial sectors [5]. Its environmental performance has been compared with that of conventional welding processes in sustainability assessments [6]. Process variants, such as bobbin-tool FSW with two shoulders [7], and joint configurations other than butt joints, such as lap joints [8], have further widened its field of application. Aluminum alloys, however, remain the main materials joined by this process [9], [10].

For these alloys, the joint strength depends closely on the welding parameters, as shown for AA2014-T6 lap joints [11] and AA2017-T351 butt joints [12]. Among the non-heat-treatable grades, AA3003 offers good corrosion resistance, formability, and thermal conductivity, and it is widely used in sheet products such as heat exchangers and cookware [13], [14]. As with other alloys, the quality of AA3003 friction stir welds depends mainly on the tool rotational speed, feed rate, and tilt angle [15]. These parameters are set independently, but together they control heat generation, the formation of the joint zones, and the resulting tensile strength and hardness [16], [17]. Strict control of these parameters is therefore essential to ensure high-performance joints.

Extensive research has been devoted to exploring new processing methods aimed at improving the mechanical properties of FSW joints in the AA3003 aluminum alloy. Goyal et al. [18] used response surface methodology to establish an empirical relationship for predicting the ultimate tensile strength of AA3003 joints. The optimal process parameters are a feed rate of 74.64 mm/min, a rotational speed of 971.77 rpm, and a tool tilt angle of 1.52°.

RSM has also been used to relate the welding parameters to the tensile behavior of friction stir welded 70/30 brass [19] and of aluminum alloy joints, including dissimilar AA3003/AA6061 [20], AA6061-T6 [21], and AA6082-T6 [22] welds. In this context, Chekalil et al. considered

feed rate, tool tilt angle, and rotational speed as input parameters for FS-welded AA3003, while yield stress, ultimate tensile strength, and rupture strength were treated as outputs. A rotational speed of 1425 rpm, a feed rate of 400 mm/min, and a tool tilt angle of 1.3° resulted in an efficiency of 75% [15]. Dellal et al. [23] identified the parameters that most affected the strength of AA3003 joints made by friction stir lap welding (FSLW). The highest rupture load, about 9 kN, was obtained for a double-lap joint welded at 1000 rpm and 250 mm/min.

Abnar et al. [24] studied the effect of the heat input generated during FSW of the AA3003 alloy on the evolution of the microstructure and the mechanical properties of the joints by varying the ratio between the rotational speed and the feed rate (N/S). It was observed that, as the rotational speed increases at a constant feed rate, the heat input becomes much greater and the grains grow considerably. Lowering the feed rate at a constant rotational speed caused a smaller rise in heat input and therefore more moderate grain growth. As a result, the hardness of the stir zone decreased more markedly at high rotational speeds.

Tan et al. [25] showed that lowering the ambient temperature during underwater FSW of AA3003 refined the recrystallized grains, and they related the yield strength of the joints to this grain size.

Other studies on AA3003 have combined mechanical tests with thermal simulation [26] or examined dissimilar joints with an aluminum matrix composite [13] and with mild steel [27]. Since heat generation links the welding parameters to these properties, the temperature field near the tool has also been measured and simulated [28], [29], [30]. Experimental designs combining N, S, and θ have already been applied to AA3003, either to optimize the tensile properties [15], [18] or to predict the maximum welding temperature [31]. To the authors' knowledge, however, these responses have not yet been analyzed together with the hardness of the weld zones within a single design. In the present study, the tensile results reported in [15] are analyzed together with temperature and hardness responses obtained for the same parameter combinations. Response surface methodology (RSM) is used to examine the individual and interaction effects of N, S, and θ on the ultimate tensile strength (σ_U), the maximum temperature (Tmax), and the hardness of the nugget zone (NZ) and the heat-affected zone (HAZ). The objective is to understand the interactions between these parameters better, identify optimal operating conditions, and establish an experimental database useful for process modeling and optimization.

2. Experimental procedure

Friction stir welds were performed on a vertical milling machine using a friction stir welding tool made of X210Cr12 steel with a tensile strength of σm = 870 MPa. The tool material and design were selected on the basis of preliminary tests reported by Chekalil et al. [15]. The geometry adopted, as shown in Figure 1, is that of a conical pin with the following dimensions: a lower diameter d = $5mm$, an upper diameter D = 6.8 mm, and a length of 1.7 mm, with a concave shoulder having an angle of 3° and a diameter of 19.5 mm.

Two plates made of 3003 aluminum alloy, measuring 210 mm × 110 mm and 2 mm thick, were secured with mechanical clamps and then butt-joined in the rolling direction using friction stir welding (FSW). During the process, temperature changes were measured using Type K thermocouples positioned 10 mm from the central axis and secured with Thermigrease TG 20033 thermal paste. In the remainder of this study, Tmax denotes the maximum temperature read from the temperature-time curve recorded by the thermocouple located 10 mm from the weld centerline. It therefore characterizes the thermal cycle at this location and does not represent the peak temperature in the nugget or at the tool-workpiece interface.

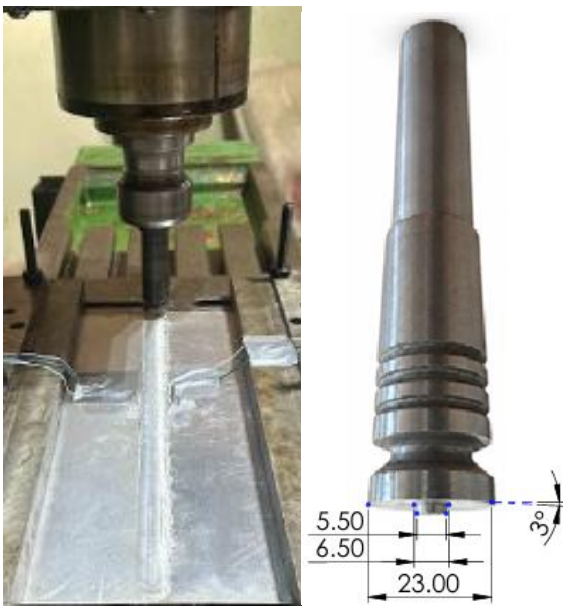


Figure 1. Configuration and FSW tool

The mechanical properties of the FSW joint made of 3003 aluminum alloy were determined by tensile tests performed on an INSTRON 8500 servo-hydraulic testing machine with a capacity of ± 100 kN (Figure 2). The ultimate tensile stress was determined from the maximum load recorded during each test. Microhardness measurements were taken perpendicular to the weld axis, with measurements taken every millimeter. These tests were performed using a semi-

automatic microhardness tester (FUTURE-TECK FM-800) with a Vickers indenter under a test load of 200 g, connected to a microcomputer that enables automatic microhardness measurement using appropriate software. The hardness values of the weld core (NZ) and the heat-affected zone (HAZ) were obtained by calculating the average of the measurements taken in the corresponding regions of the joint.



Figure 2. Tensile test of the dumbbell-shaped specimen measured by the extensometer

Figure 3 shows the sample extraction for monotonic tensile and microhardness tests; the test specimens were cut using a waterjet.

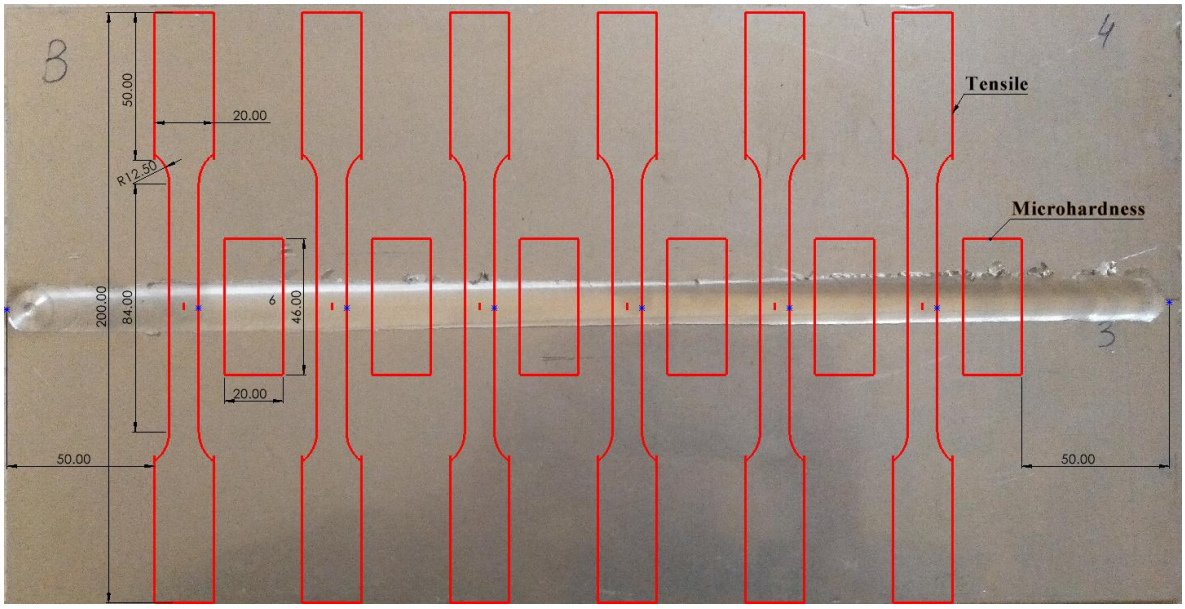


Figure 3. Sample extraction (actual dimensions in mm)

The stress-strain curve for AA3003 aluminum alloy is shown in Figure 4. This test made it possible to determine the main mechanical properties summarized in Table 1.

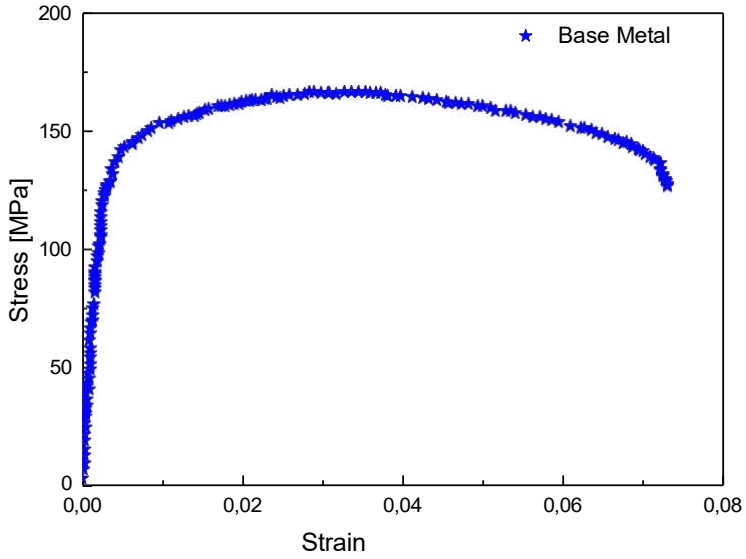


Figure 4. Tensile test curves for 3003 aluminum alloy.

Table 1. Mechanical Properties of the Base Metal.

Microhardness (HV)	σ_e *(MPa)*	σ_U *(MPa)*	σ_m *(MPa)*	A	E (GPa)	Melting Point (°C)
55	110	160	127	5.6	60	650

A COXEM scanning electron microscope (SEM) with a voltage of 15 kV and a magnification of x2000 was used for the physicochemical analysis of 3003 aluminum alloy. Table 2 shows the chemical composition of the material used.

Table 2. Chemical Composition of 3003 Aluminum Alloy.

Element	Al	Mn	Si	Fe	Cu	Ti	Zn	Mg	Cr
%	96.7	1.3	0.9	0.9	0.13	0.1	0.03	0	0

3. Design of experiments and RSM modeling

The optimization was performed using a full factorial design with three factors: rotational speed, feed rate, and tool tilt angle at three levels (-1, 0, +1). Table 3 below lists the values of each parameter for each level. The values of these parameters are determined by the machine's capacity and premature tool wear.

Table 3. Parameter Values for Each Level.

Parameters	Low level (-1)	Middle level (0)	High level (+1)
Rotational speed (rpm)	1000	1500	2000
Feed rate (mm/min)	200	300	400
Tool tilt angle (°)	0.5	1.5	2.5

The experimental design matrix was generated using Design-Expert 13 software [32]. The results of the 30 tests are summarized in Table 4, where each row corresponds to a test whose value represents the average of three replicates conducted under the same conditions. The σ_U values in Table 4 are those reported in [15] for the same parameter combinations; in the present work, they are analyzed together with the temperature and hardness responses.

Table 4. Matrix of experiments.

No.	N (rpm)	S (mm/min)	θ (°)	σ_U (MPa)	NZ (HV)	HAZ (HV)	Tmax (°C)
1	1000	200	0.5	128	48.66	41.85	207
2	1500	200	0.5	123.2	40.72	34.6	242
3	2000	200	0.5	123.8	38	34.5	323
4	1000	300	0.5	103.7	54.02	45.1	210
5	1500	300	0.5	102.8	45.84	36.4	208
6	2000	300	0.5	97.8	45.62	38.3	253
7	1000	400	0.5	125.9	48	44.1	184
8	1500	400	0.5	109.8	43	36.1	200
9	2000	400	0.5	98.4	41.04	34.3	249
10	1000	200	1.5	100.3	47.56	44.55	201
11	1500	200	1.5	118.4	39.18	38.5	246
12	2000	200	1.5	121.1	37.58	36.4	263
13	1000	300	1.5	94.7	46	39.95	199
14	1500	300	1.5	107.4	40.26	34.2	211
15	2000	300	1.5	107.6	38	38.05	252
16	1000	400	1.5	109.1	44.06	39.35	203
17	1500	400	1.5	115.6	40.66	35.85	259
18	2000	400	1.5	127.8	36.5	33.05	273
19	1000	200	2.5	92.5	43.72	34.2	249
20	1500	200	2.5	100.1	39.2	31.8	342
21	2000	200	2.5	120.1	36.14	34.5	368
22	1000	300	2.5	73.1	42.72	37.8	236
23	1500	300	2.5	106.8	41.12	32.65	300
24	2000	300	2.5	110.6	36.42	30.95	333
25	1000	400	2.5	95.8	36.06	33.85	216
26	1500	400	2.5	113.6	33.28	27.15	296
27	2000	400	2.5	120	31.96	30.25	309

28	1500	300	1.5	108.5	41.82	38.1	196
29	1500	300	1.5	108.2	41.82	38.1	197
30	1500	300	1.5	107.9	41.82	38.1	197

4. Results and Discussion

Polynomial regression models relating Tmax, σ_U, and the NZ and HAZ hardness to N, S, and θ were fitted with Design-Expert software. RSM was preferred to data-driven approaches, such as the hybrid deep learning model used to predict the ultimate tensile strength of FSW joints [33], because it provides explicit equations from a limited number of runs and shows the effect of each factor directly. The models contain linear, quadratic, and two-factor interaction terms, together with the cubic interaction terms that a three-level design can estimate. The fitted equations, expressed in terms of the actual factor values, are:

$$NZ = 79.74104 - 0.086486 \cdot N + 0.159283 \cdot S - 4.75722 \cdot \theta + 0.000128 \cdot N \cdot S + 0.014365 \cdot N \cdot \theta - 0.057508 \cdot S \cdot \theta + 0.000024 \cdot N^2 - 0.000403 \cdot S^2 + 0.349167 \cdot \theta^2 - 5.5 \cdot 10^{-7} \cdot N \cdot S \cdot \theta - 3.24 \cdot 10^{-8} \cdot N^2 \cdot S - 5.46667 \cdot 10^{-6} \cdot N^2 \cdot \theta - 2.4 \cdot 10^{-8} \cdot N \cdot S^2 + 0.00118 \cdot N \cdot \theta^2 + 0.000095 \cdot S^2 \cdot \theta - 0.00575 \cdot S \cdot \theta^2 \quad (1)$$

$$HAZ = 61.6388 - 0.055047 \cdot N + 0.092649 \cdot S + 12.77257 \cdot \theta + 0.000031 \cdot N \cdot S + 0.009687 \cdot N \cdot \theta - 0.062479 \cdot S \cdot \theta + 0.000014 \cdot N^2 - 0.000096 \cdot S^2 - 6.42813 \cdot \theta^2 - 3.625 \cdot 10^{-6} \cdot N \cdot S \cdot \theta + 1.66667 \cdot 10^{-9} \cdot N^2 \cdot S - 1.86667 \cdot 10^{-6} \cdot N^2 \cdot \theta - 6.33333 \cdot 10^{-8} \cdot N \cdot S^2 - 0.000233 \cdot N \cdot \theta^2 + 0.000026 \cdot S^2 \cdot \theta + 0.013917 \cdot S \cdot \theta^2 \quad (2)$$

$$\sigma_U = 370.41667 - 0.061967 \cdot N - 1.45801 \cdot S - 144.99861 \cdot \theta + 0.000205 \cdot N \cdot S + 0.067675 \cdot N \cdot \theta + 0.294375 \cdot S \cdot \theta + 7.91667 \cdot 10^{-6} \cdot N^2 + 0.002457 \cdot S^2 + 21.725 \cdot \theta^2 + 5 \cdot 10^{-5} \cdot N \cdot S \cdot \theta - 1.13333 \cdot 10^{-8} \cdot N^2 \cdot S - 0.000012 \cdot N^2 \cdot \theta - 4.9 \cdot 10^{-7} \cdot N \cdot S^2 - 0.00885 \cdot N \cdot \theta^2 - 0.000328 \cdot S^2 \cdot \theta - 0.041333 \cdot S \cdot \theta^2 \quad (3)$$

$$T_{max} = 442.68229 - 0.179028 \cdot N + 0.366667 \cdot S - 404.39583 \cdot \theta - 0.001329 \cdot N \cdot S + 0.204917 \cdot N \cdot \theta + 0.829583 \cdot S \cdot \theta + 0.000179 \cdot N^2 - 0.001356 \cdot S^2 + 75.39583 \cdot \theta^2 + 0.000062 \cdot N \cdot S \cdot \theta - 9 \cdot 10^{-8} \cdot N^2 \cdot S - 0.000097 \cdot N^2 \cdot \theta + 2.31667 \cdot 10^{-6} \cdot N \cdot S^2 + 0.027167 \cdot N \cdot \theta^2 - 0.000175 \cdot S^2 \cdot \theta - 0.2725 \cdot S \cdot \theta^2 \quad (4)$$

Figure 5 compares the predicted and measured values for the 30 runs used to fit the models. For all responses, the points lie close to the 45° line, with coefficients of determination (R^2) of 0.96 for Tmax and NZ hardness, 0.93 for σ_U, and 0.90 for HAZ hardness.

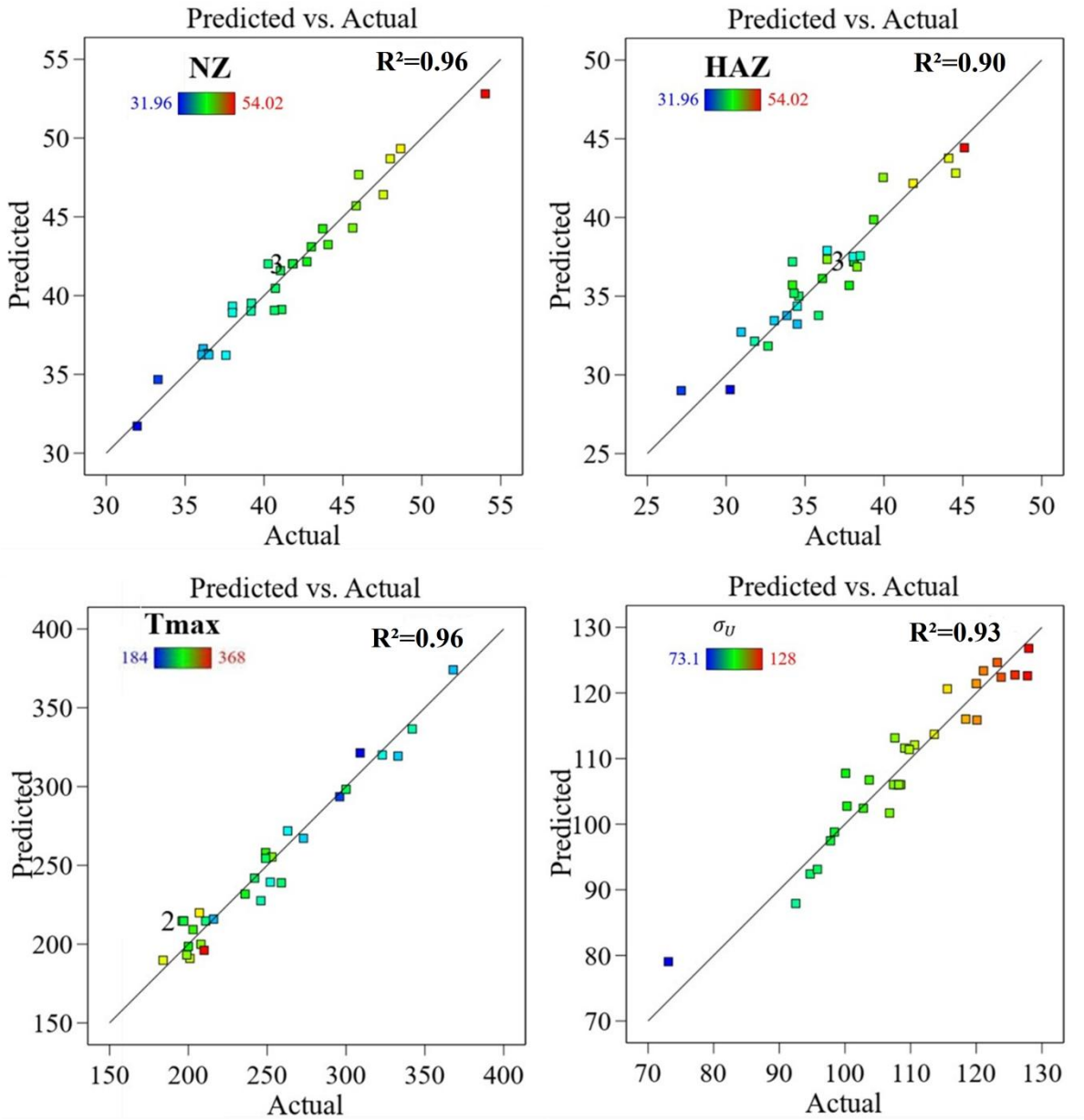


Figure 5. Experimental and Predicted Values.

Some scatter nevertheless remains around the diagonal, particularly for HAZ hardness and for the lowest σ_U value (73.1 MPa, run 22), which the model overestimates. Across the design, σ_U ranged from 73 to 128 MPa, which shows that the tensile strength of the joints is highly sensitive to the welding parameters. Hardness responds to the thermomechanical cycle produced during welding and is therefore used here as an indirect indicator of microstructural change. The lower R^2 of the HAZ model may partly reflect the averaging of hardness values over a region where hardness changes rapidly with distance from the weld center.

It is necessary to analyze the individual and interaction effects of the parameters on each response to understand the behavior of the joint and to highlight the complexity of thermomechanical coupling during FSW.

4.1. Individual effect of process parameters

Figures 6 (a, b, and c) illustrate, respectively, the individual influence of the rotational speed (N), the feed rate (S), and the tool tilt angle (θ) on the average NZ hardness, with the other two factors held constant.

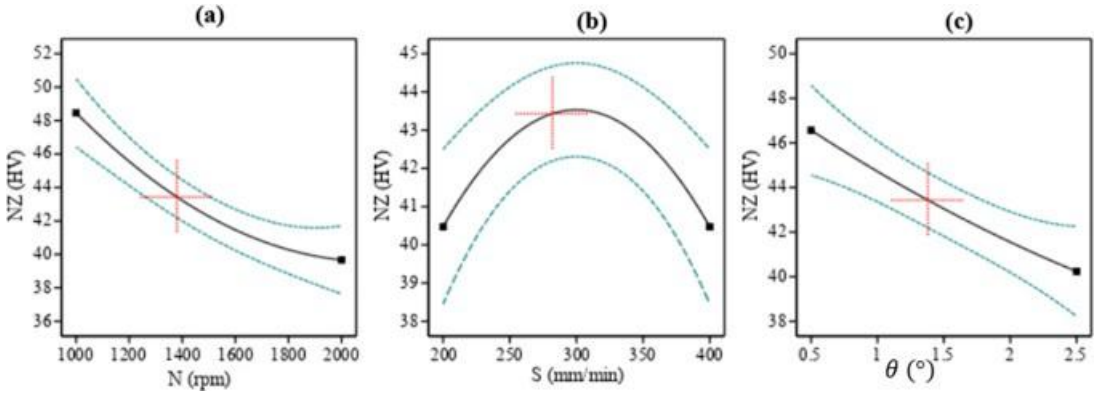


Figure 6. Effect of welding parameters on nugget zone hardness.

Figure 6 (a) shows a significant decrease in core hardness as the rotational speed increases. At 1000 rpm, hardness is at its maximum (≈ 48 HV), whereas it drops to approximately 39 HV at 2000 rpm. Doubling the rotational speed therefore lowers the NZ hardness by about 17%. A likely explanation is the higher frictional heat input at high rotational speed [2], which raises the weld temperature [34] and can promote recovery and grain growth in the nugget. Since grain size and dislocation density were not measured here, this mechanism remains to be confirmed.

Figure 6 (b) shows that the NZ hardness first increases with feed rate, from about 40.5 HV at 200 mm/min to a maximum of about 43.5 HV near 300 mm/min, and then falls back to about 40.5 HV at 400 mm/min. The initial increase agrees with the finer nugget grains reported at higher welding speeds for a high-strength Al-Zn-Mg-Cu alloy [35], although that alloy is strengthened by precipitation, unlike AA3003. A plausible explanation for the whole curve is that the longer thermal exposure at low feed rates favors grain growth, whereas the shorter stirring time at high feed rates may produce less uniform material flow. Within the tested range, a feed rate of about 300 mm/min therefore gives the highest NZ hardness.

Figure 6 (c) shows a trend similar to that of rotational speed: the NZ hardness decreases steadily from about 46.5 HV at 0.5° to about 40 HV at 2.5°. A larger tilt angle increases the contact

pressure of the shoulder and, consequently, the heat generated, as shown by the Tmax results in Figure 9 (c). The lower hardness at large tilt angles is therefore consistent with additional heating, which may favor recrystallization and grain growth in the nugget.

Figure 7 shows that the HAZ hardness varies nonlinearly with each welding parameter. Unlike the NZ, the HAZ is not stirred by the tool, so its hardness depends mainly on the thermal cycle it experiences.

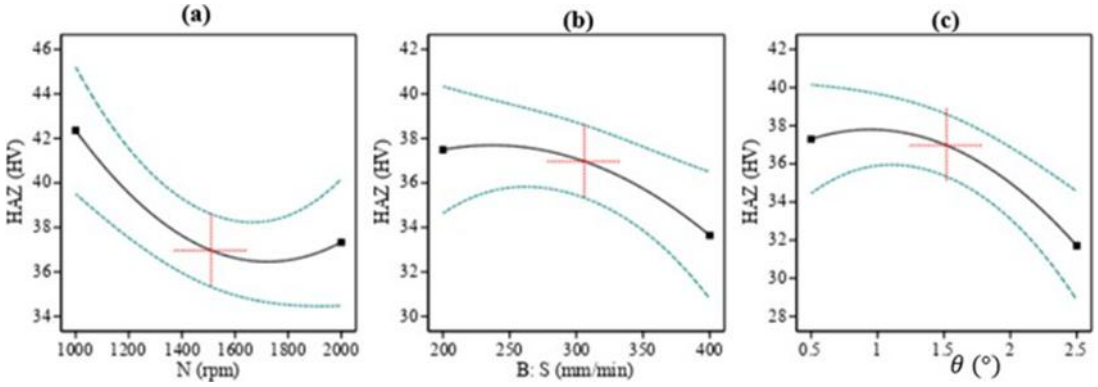


Figure 7. Effect of welding parameters on hardness in the HAZ

In Figure 7 (a), the HAZ hardness decreases from about 42.5 HV at 1000 rpm to a minimum of about 36.5 HV between 1600 and 1700 rpm and then rises slightly, to about 37 HV, at 2000 rpm. At low rotational speed, the smaller heat input limits recovery and recrystallization in the HAZ, so that more of the work hardening of the base metal is retained. As the rotational speed increases, the heat generated mainly by friction between the shoulder and the workpiece softens the HAZ. The slight rise near 2000 rpm lies within the confidence band of the model and should not be overinterpreted.

Figure 7 (b) shows that the HAZ hardness changes little between 200 and 300 mm/min (about 37 to 38 HV) and then decreases to about 33.5 HV at 400 mm/min. This decrease is not what heat input alone would predict, because a higher feed rate lowers the heat input per unit length and should reduce HAZ softening. The model does predict a rise in Tmax between 300 and 400 mm/min (Figure 9 (b)), and the thermocouple was located near the outer edge of the shoulder (radius 9.75 mm), in or close to the HAZ. HAZ softening at 400 mm/min may therefore follow the local thermal cycle rather than the nominal heat input. However, this rise in Tmax was not observed in all runs, as discussed with Figure 9, and the higher Tmax at 200 mm/min did not lower the HAZ hardness. The effect of feed rate on HAZ hardness thus remains only partly explained.

The effect of tilt angle is shown in Figure 7 (c). The HAZ hardness remains between about 37 and 38 HV up to 1.5°, with a weak maximum near 1°, and then falls to about 31.5 HV at 2.5°. This drop matches the steep rise in Tmax above about 1.5° (Figure 9 (c)), which supports the view that the additional frictional heat produced at large tilt angles is the main cause of HAZ softening.

Figure 8 shows the effect of the welding parameters on the ultimate tensile strength (σ_U) of the AA3003 joints, which is used here as the main indicator of their load-bearing capacity.

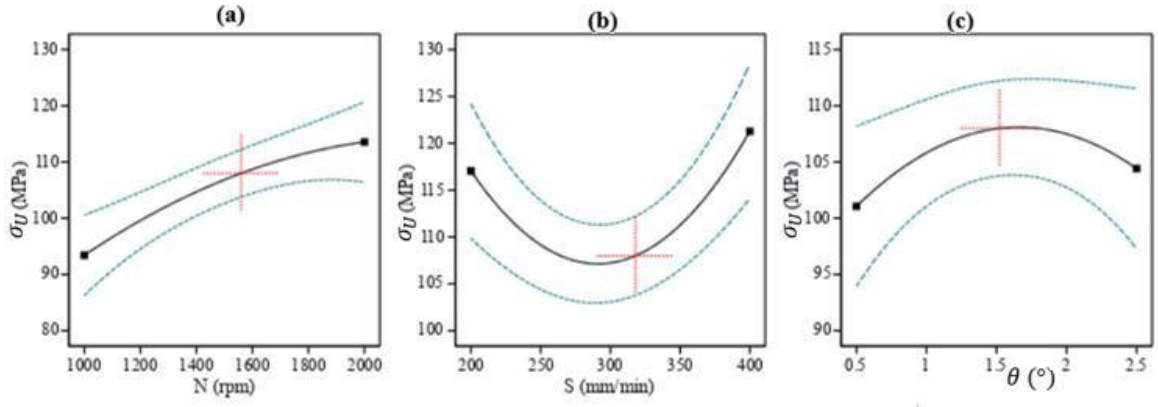


Figure 8. Effect of welding parameters on ultimate tensile strength.

In Figure 8 (a), σ_U increases steadily with rotational speed, from about 93 MPa at 1000 rpm to about 113 MPa at 2000 rpm. A likely reason is that the lower heat input at 1000 rpm is not sufficient for complete material flow and bonding, although no defect analysis was carried out to confirm this. Takhakh and Abdullah [36] also found that the efficiency of AA3003-H14 joints depended strongly on rotational speed, with the best efficiency at 1500 rpm and 80 mm/min. This trend is opposite to that of hardness (Figures 6 (a) and 7 (a)): a higher rotational speed softens the NZ and HAZ but improves σ_U. Within the tested range, σ_U therefore appears to depend more on the quality of bonding than on the hardness of the weld zones.

Regarding the effect of feed rate on σ_U, Figure 8 (b) illustrates this variation. Analysis of this figure shows that as the feed rate S increases, the ultimate tensile strength first decreases, then begins to increase, reaching a maximum value at feed rates of 200 mm/min and 400 mm/min. The minimum, about 107 MPa, occurs near 300 mm/min, and the highest value, about 121 MPa, is predicted at 400 mm/min. The same feature was found in [15], whose tensile data are reanalyzed here, and it is examined further with the interaction plots in Figure 13.

Figure 8 (c) shows that σ_U follows an inverted parabola with tilt angle, rising from about 101 MPa at 0.5° to a maximum of about 108 MPa near 1.5° and then decreasing to about 104.5 MPa at 2.5°. A small tilt angle gives limited forging by the trailing edge of the shoulder, which may leave the stirred material less well consolidated, whereas a large angle increases the heating (Figure 9 (c)) and may soften the joint. Studies on other aluminum alloys and joint types have also shown that the tilt angle strongly affects joint quality, for example in AA2014-T6 lap joints [37], in AA2219 plates, where intermediate angles of 1° to 2° avoided defects [38], in Al-Mg-Si T-joints [39], and in Al-Cu-Li alloys [40]. Because the best angle depends on the alloy, thickness, tool, and joint type, the optimum near 1.5° found here applies only to the present conditions. A related observation was made for friction stir spot welded AA3003-H12, where the plunge depth, which also controls the shoulder contact, had a larger effect on the tensile shear load than the rotational speed and dwell time [41].

To improve the performance of the joints and ensure optimal quality, it is necessary to identify, model, and optimize, among other factors, the heat generated during the FSW process. Temperature is an important factor as it directly affects the microstructures and mechanical properties of the welded joints. Analysis of the effect of rotational speed, feed rate, and tool tilt angle on the evolution of the maximum temperature produced during the welding of a 3003 aluminum alloy is shown in Figure 9.

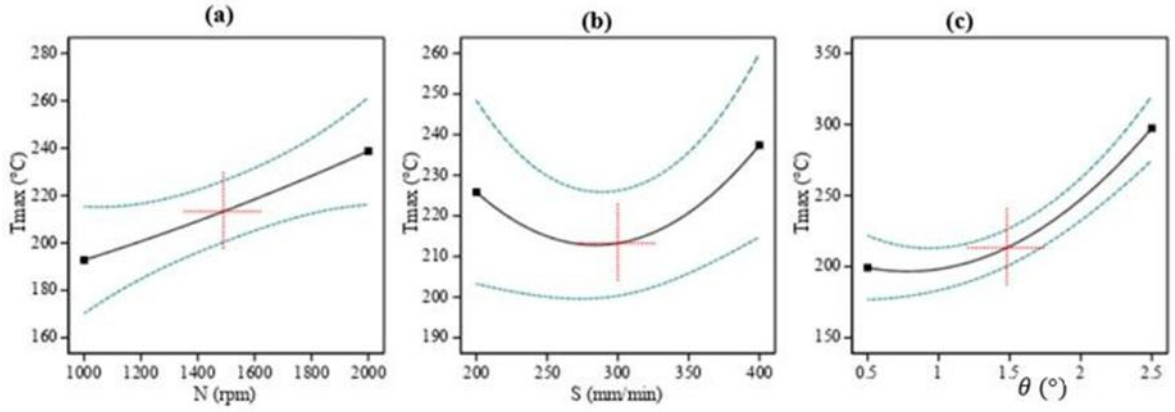


Figure 9. Effect of welding parameters on Tmax

Figure 9 (a) shows that Tmax increases almost linearly with rotational speed, from about 193 °C at 1000 rpm to about 238 °C at 2000 rpm, that is, by about 23% when N is doubled. A higher rotational speed increases the frictional heat generated between the tool and the plates. Kilic et al. [2] also identified rotational speed as a major contributor to heat generation in FSW, and Sabry et al. [34] found that the weld temperature increased with rotational speed in both

conventional and underwater FSW. The effect of feed rate on Tmax (Figure 9 (b)) is nonlinear, with a minimum of about 213 °C near 300 mm/min and higher values at 200 mm/min (about 226 °C) and 400 mm/min (about 237 °C). The higher temperature at low feed rate is expected, because the tool stays longer over each point of the joint and the heat input per unit length increases. The predicted rise at 400 mm/min is less certain: in Table 4, Tmax at 400 mm/min exceeded that at 300 mm/min in only three of the nine comparable combinations of N and θ, so this part of the curve should be interpreted with caution. The link between temperature and strength is therefore not straightforward. The higher temperature at 200 mm/min may favor material flow and bonding, in agreement with the high σ_U obtained at this feed rate (Figure 8 (b)), but the equally high σ_U at 400 mm/min cannot be attributed to temperature alone. Macrographic and fractographic observations would be needed to clarify this point.

The tilt angle has the strongest effect on Tmax (Figure 9 (c)). Tmax changes little between 0.5° and about 1° and then rises steeply, reaching about 297 °C at 2.5°. A larger tilt angle is expected to increase the shoulder pressure and the contact area on the trailing side of the tool, which intensifies frictional heating and plastic deformation at the tool-workpiece interface. Within the tested ranges, the tilt angle is therefore the main factor controlling Tmax, followed by the rotational speed.

4.2.Interacting effect of process parameters

We decided to broaden the scope of our study by considering the interaction between two factors; this allows us to visualize the output parameters on a three-dimensional (3D) graph. The example in Figure 10 represents the variation in hardness within the nugget zone as a function of the two factors N and S. The projection of the surface onto the plane results in curves visualized in Figures 11, 12, 13 and 14, commonly referred to as “Iso curves”.

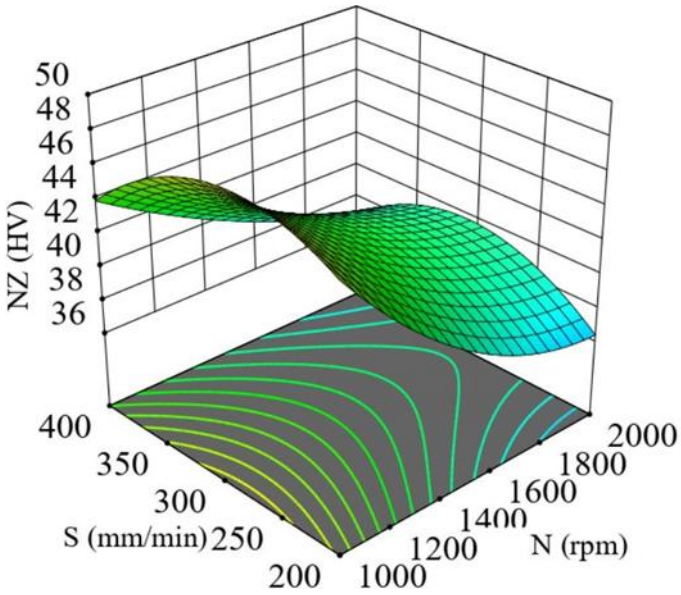


Figure 10. 3D variation of hardness in the nugget zone as a function of N and S.

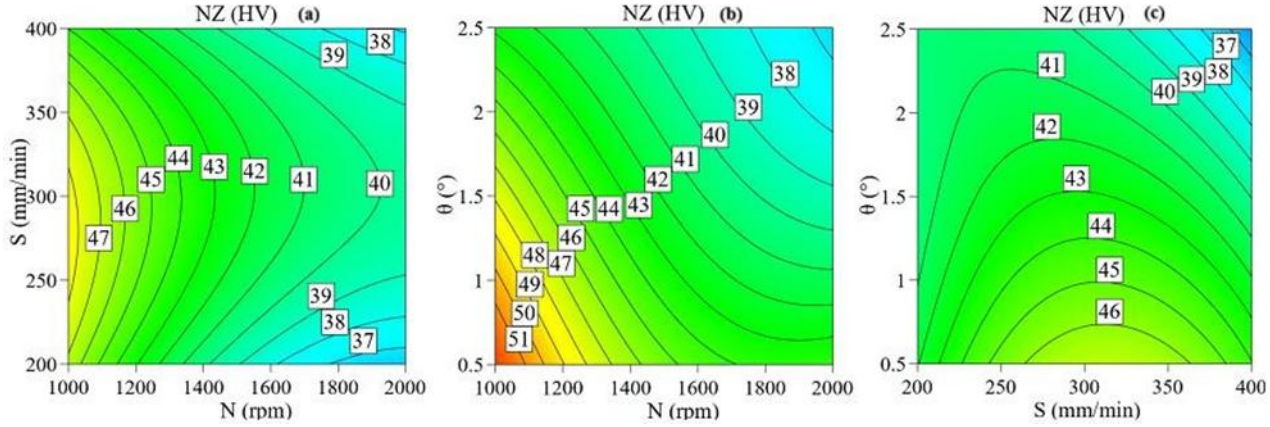


Figure 11. Hardness variation in the nugget zone as a function of welding parameters.

Figure 11 (a) shows that the lowest hardness values were recorded for the maximum values of N = 2000 rpm and the extreme values of S (200 and 400 mm/min). It should also be noted that the best hardness values for the weld core were obtained for a ratio N/S between 2.85 and 4. A likely explanation is that a high rotational speed generates more frictional heat, which coarsens the recrystallized grains in the nugget and lowers the hardness according to the Hall–Petch relation. El Rayes et al. [42] reported such a relation between stir-zone grain size and hardness in AA5754, but grain size was not measured in the present study, so this explanation remains to be verified.

Analysis of Figure 11 (b) reveals that the increase in hardness in the core is promoted by decreases in N and θ. In contrast, the lowest hardness is observed for the maximum values of these two factors.

Finally, Figure 11 (c) illustrates the variation in core hardness as a function of the factors θ and S. In this case, the highest hardness values, approaching 46 HV, are recorded for a low value of θ and feed rates between 250 and 350 mm/min. In contrast, the hardness reaches its lowest values when a feed rate close to 400 mm/min is combined with a tilt angle of 2° to 2.5°.

Reported effects of feed rate on nugget hardness depend on the material and welding conditions. El Rayes et al. [42] observed finer stir-zone grains and a small increase in hardness when the travel speed of AA5754 welds was increased at constant rotational speed. In dissimilar AA2024-T3/AA7475-T761 joints, Delijaicov et al. [43] attributed the hardness changes to thermal softening, recrystallization, and precipitation, all of which depend on the welding parameters. For Al/Cu butt joints, Elmetwally et al. [44] obtained the highest strength at low travel speed and high rotational speed. In the present AA3003 joints, the low NZ hardness at high feed rate and large tilt angle does not follow a simple travel-speed trend. At θ = 2.5°, Table 4 shows that both Tmax and NZ hardness were lower at 400 mm/min than at 200 mm/min. NZ hardness is therefore not controlled by the measured peak temperature alone; less complete material flow at high feed rate may also contribute, but this needs microstructural verification.

The interaction effects on HAZ hardness are shown in Figure 12.

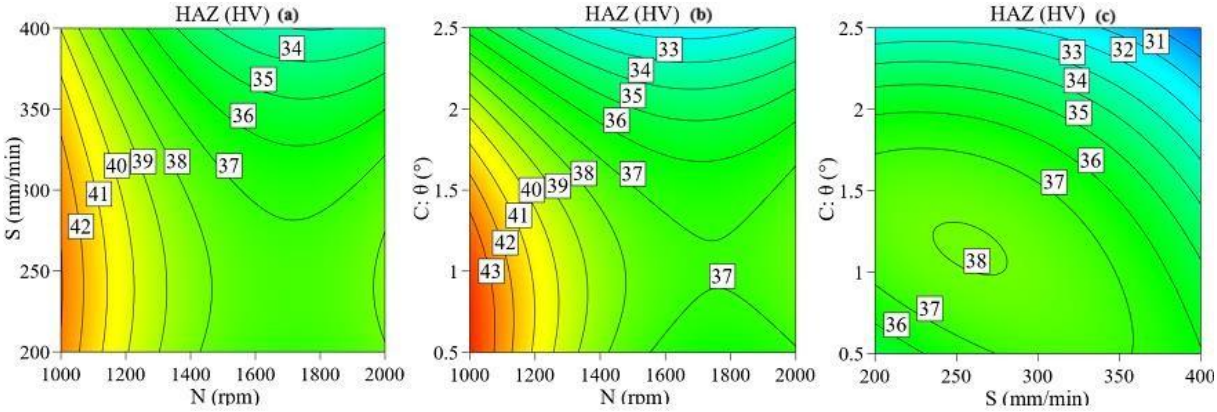


Figure 12. Variation in hardness in the HAZ as a function of welding parameters

Figure 12 (a) shows that the highest HAZ hardness (above 42 HV) is obtained at low rotational speed (N ≈ 1000 rpm), mainly for feed rates below about 300 mm/min. Although the N/S ratio is high for these combinations, the low rotational speed limits the frictional heat. In Table 4, Tmax at 1000 rpm and 200 mm/min remained between 201 and 249 °C, below the middle of the measured range (184 to 368 °C), which is consistent with limited softening of the work-hardened HAZ. Conversely, at high rotational speeds (N > 1600 rpm), a drop in hardness is

observed regardless of S (isolines at 37 HV). This phenomenon highlights the predominant influence of the thermal effect of rotational speed on the preservation of hardness.

Analysis of curve 12 (b) reveals a region of maximum hardness (HAZ > 43 HV) at low rotational speeds (N ≈ 1000 rpm) combined with small tilt angles (θ < 1°). This combination, which generates minimal heat input (reduced axial friction and forging), limits annealing of the AA3003, so that more of the work-hardened state is retained in the HAZ. It is thus observed that an increase in N and θ leads to a rapid drop in hardness (isolines falling to as low as 33 HV). This indicates that an increase in energy input, whether thermal (related to N) or mechanical friction (related to θ), results in softening of the alloy.

The interaction curve between the inclination angle and the feed rate (Figure 12 (c)) shows that the maximum hardness (HAZ > 38 HV) is achieved at low angles (θ < 1.5°) and low feed rates (S < 275 mm/min). This combination of parameters minimizes thermal and mechanical stresses, thereby limiting the annealing softening effect. However, an increase in θ beyond 1.5°, even at low feed rates, results in a significant drop in hardness (isolines falling to 31 HV). This suggests that the increase in friction energy induced by the angle has a more detrimental impact on hardness than variations in feed rate.

Figure 13 illustrates the variation of σ_U depending on the interaction of welding parameters.

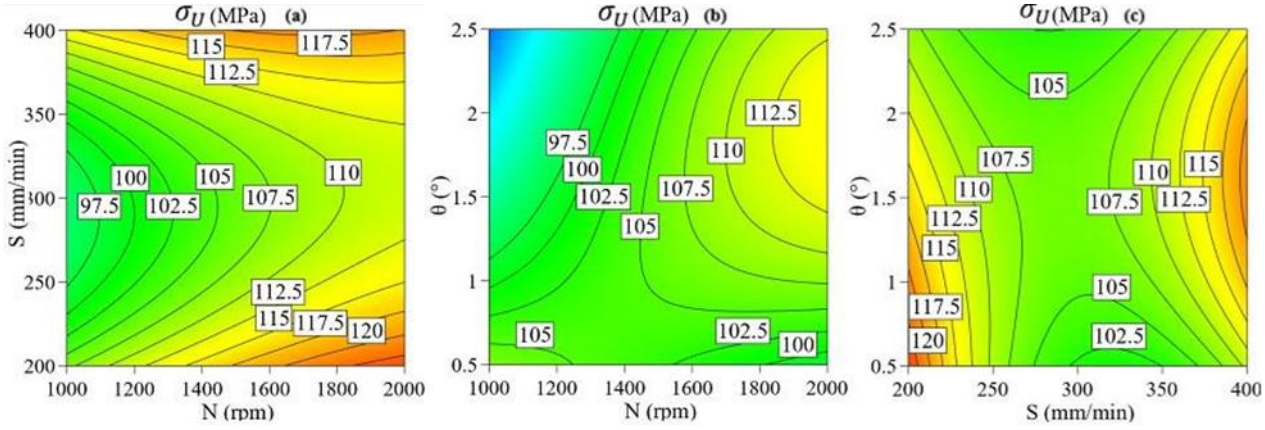


Figure 13. Variation of σ_U as a function of welding parameters

Figure 13 (a) shows the effect of the two factors S and N acting simultaneously on σ_U, ranging from their minimum to their maximum values, while the third factor (θ) is held constant. Analysis of the graph suggests that σ_U takes on maximum values in two interaction intervals; the first interval corresponds to low values of S = 200 mm/min with N ranging from 1700 to 2000 rpm, and the second corresponds to high values of S = 400 mm/min, while N remains

within the range of 1700 to 2000 rpm. It is also worth noting that the best values of σ_U for the welded joint are equal to 81% of those of the base metal. Consequently, high σ_U values require N between 1700 and 2000 rpm combined with either a low or a high feed rate. The high-feed-rate region is consistent with the optimum feed rate of 400 mm/min previously obtained for these tensile data [15]. The low-feed-rate region agrees with the observation of Pourali et al. [45] that low travel speed and high rotational speed increased the shear strength of dissimilar Al1100/St37 lap joints, although that study concerns a different material combination and joint type.

The analysis of the combined effect of N and θ, for a constant S, is shown in Figure 13 (b). It can be seen that σ_U reaches an optimum for values of θ and N ranging, respectively, between 1.5 - 2.5° and 1600 - 2000 rpm. In this optimal configuration, the strength of the welded joint is 78% of that of the base metal, which is close to the joint efficiency of 75% reported in [15].

Analysis of the contour diagram for σ_U, performed at a constant rotational speed, highlights the significant interaction between θ and S (Figure 13 (c)). Two regions of high strength can be distinguished. At low feed rates (about 200 to 250 mm/min), the highest values, close to 120 MPa, are obtained with small tilt angles (0.5° to 1°). At high feed rates (about 375 to 400 mm/min), high strength (above 115 MPa) requires a larger tilt angle, between about 1° and 2°. A possible interpretation is that the longer stirring time at low feed rate allows good consolidation with limited forging, whereas at high feed rate a larger tilt angle is needed to increase the forging action and the heat input. Conversely, a drop in performance is observed in the intermediate range ($S \approx$ 300 - 350 mm/min, low θ), possibly resulting from an unfavorable combination: insufficient interaction time coupled with inadequate dynamic confinement, leading to incomplete consolidation.

This final stage of the analysis is devoted to studying the interaction effect of welding parameters on Tmax (Figure 14).

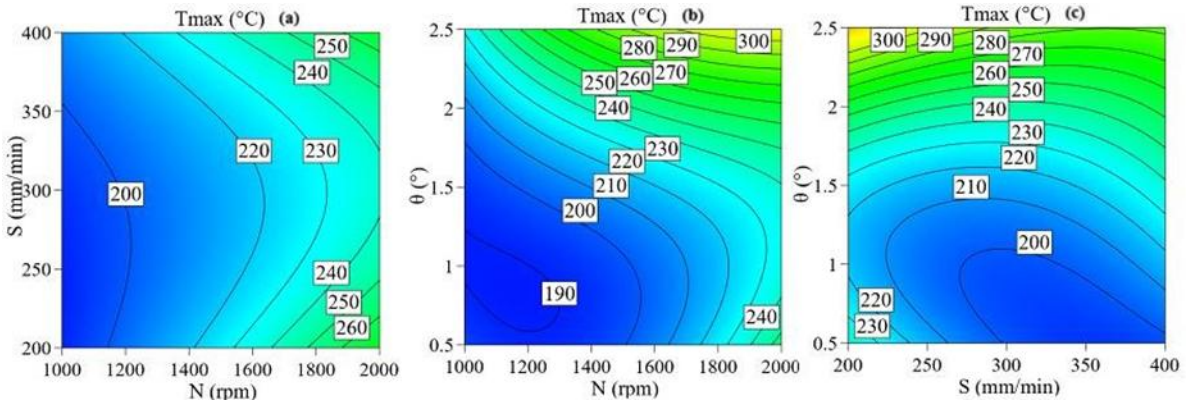


Figure 14. Variation of Tmax as a function of welding parameters

In Figure 14 (a), with the tool tilt angle (θ) held constant, Tmax reaches its highest values in the interaction zone corresponding to high rotational speeds (N = 1700 - 2000 rpm) combined with feed rates (S) in the ranges of 200 - 250 mm/min and 375 - 400 mm/min. The lowest values, below about 200 °C, occur near 1000 rpm over the whole feed-rate range.

Figure 14 (b) shows that maximum temperatures occur when the rotational speed ranges between 1300 and 2000 rpm and the tilt angle (θ) is between 2° and 2.5°. In contrast, the lowest temperatures are recorded at low rotational speeds (N = 1000 rpm) combined with small tilt angles (θ = 0.5° - 1.4°).

In Figure 14 (c), Tmax is highest, about 300 °C, when a large tilt angle (above about 2.1°) is combined with a low feed rate (200 to 250 mm/min). It is lowest, about 200 °C, for tilt angles of 0.5° to 1.25° combined with feed rates of 300 to 400 mm/min.

Together, Figures 14 (a) to (c) show that Tmax is governed mainly by the tilt angle and the rotational speed, while the feed rate has a weaker, nonlinear effect that depends on the tilt angle. Higher rotational speeds and larger tilt angles increase frictional heating and plastic deformation, which raises the temperature. The interaction terms of the RSM models describe these coupled effects, which would be missed if the parameters were varied one at a time.

Taken together, the thermal and hardness results show a consistent pattern: the conditions that gave the highest Tmax (high N and large θ) also gave the lowest NZ and HAZ hardness (Figures 11, 12, and 14). This agreement suggests that the softening of both zones is controlled mainly by heat input. It does not, however, identify the mechanism, which may involve recovery, recrystallization, and grain growth and requires direct microstructural observation. Heat input is also not the only factor: Laska et al. [46] showed for AA6082 that tool geometry changed the temperature, material flow, and stir-zone grain size. In addition, the mechanical properties of

AA3003 friction stir welds change after exposure to corrosive environments [47], so the present optimum, obtained for as-welded joints, may not apply directly in service. Numerical studies have described how the temperature and strain fields develop during FSW of dissimilar aluminum alloys [48], and machine learning models have been used to predict Tmax in AA3003 welds [49]. Such approaches could complement the present measurements, which were taken at a single thermocouple position. Finally, excessive heat input at high rotational speed may cause burr formation, which is a further reason to avoid the hottest parameter combinations.

4.3. Optimal process parameters

The optimization aimed to maximize σ_U and the NZ and HAZ hardness simultaneously, with N, S, and θ kept within the tested ranges and Tmax left free within its observed range (Figure 15). Because σ_U increases with rotational speed whereas hardness decreases (Figures 6 to 8), the result is a compromise between strength and hardness.

The best solution, with an overall desirability of 0.924 (Figure 15), was obtained for a rotational speed of 1000 rpm, a feed rate of 400 mm/min, and a tool tilt angle of 0.5°. Under these conditions, the models predict a hardness of 49.2 HV in the NZ and 43.8 HV in the HAZ, a σ_U of 122.7 MPa, and a Tmax of 196 °C at the thermocouple location, close to the lowest temperature of the experimental matrix. These values correspond to about 77% of the tensile strength of the base metal (160 MPa) and to about 89% and 80% of its hardness (55 HV) in the NZ and HAZ, respectively. This parameter combination is run 7 of the design matrix, for which 125.9 MPa, 48 HV (NZ), 44.1 HV (HAZ), and 184 °C were measured, so the predicted optimum is supported by a tested condition. However, all three factors lie at the limits of the investigated ranges, which means that better combinations may exist outside the tested domain.

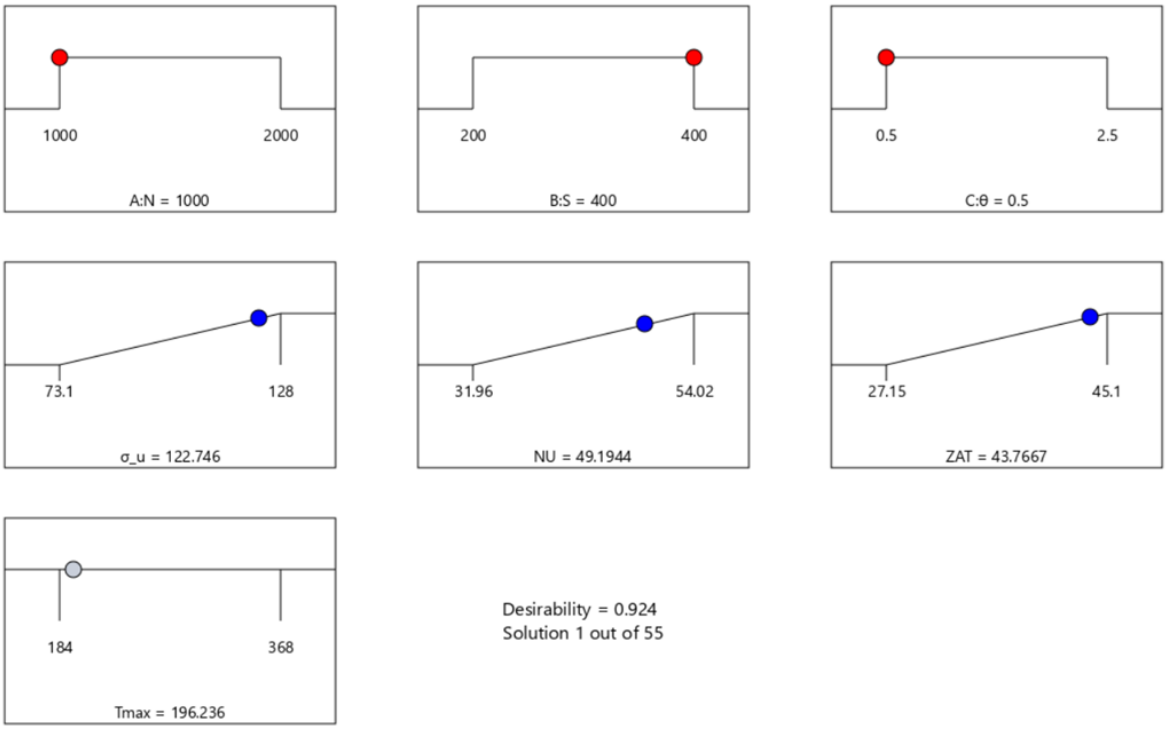


Figure 15. Optimal FSW welding conditions.

Eight additional welds, which were not used to fit the models, were produced within the investigated parameter ranges to validate them.

Figure 16 compares the predicted and measured values for these validation tests. For all four responses, the points follow the 45° line, which shows that the models reproduce the trends of the measured data. Most points, however, lie slightly above the line, which indicates that the models tended to underestimate the measured values in these tests.

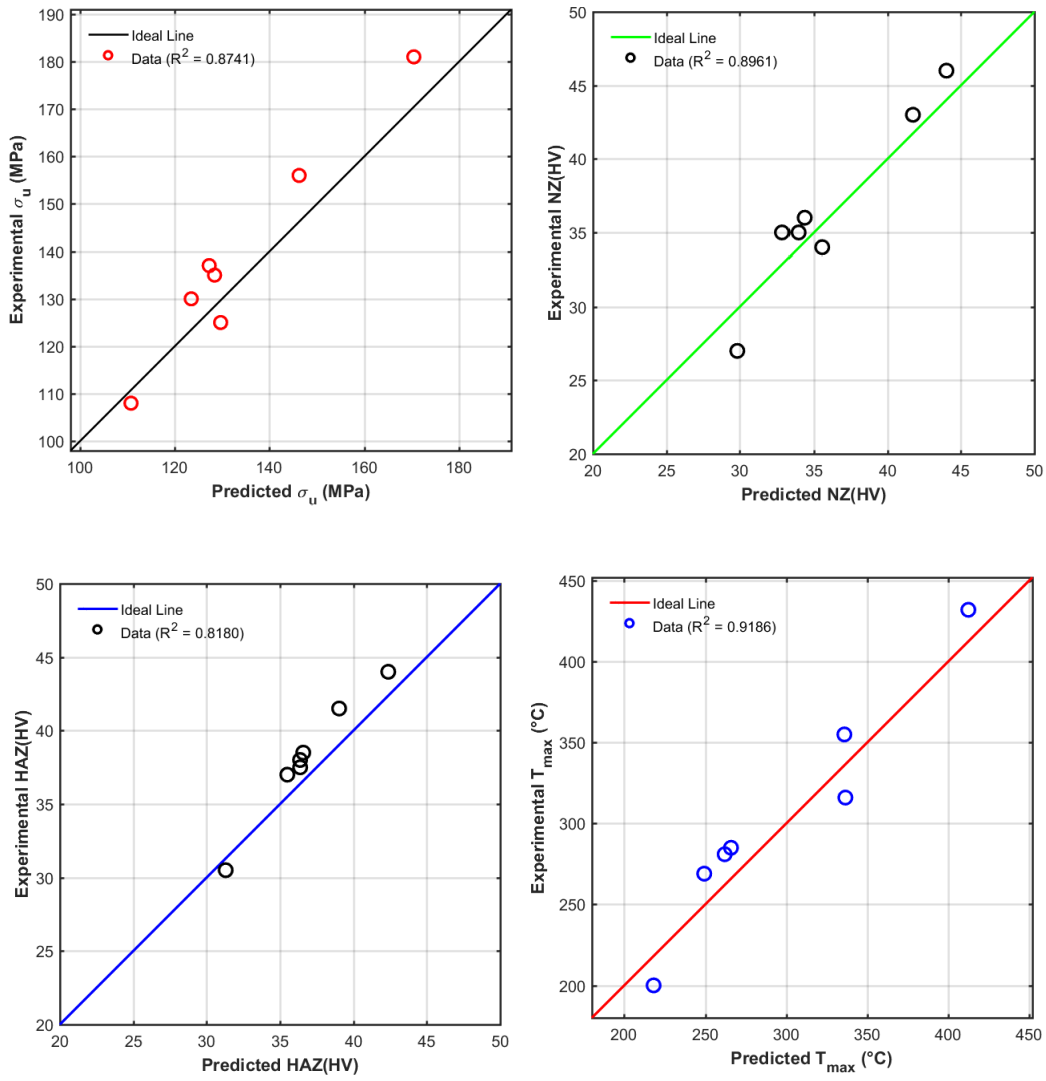


Figure 16. Correlation between predicted values and experimental values for the validation set.

Table 5 gives the root mean square error (RMSE), the mean absolute error (MAE), and R^2 obtained for the validation set.

Table 5. Prediction performance of the models for the validation set

Model	RMSE	MAE	R^2
σ_U	7.72	7.23	0.8741
NZ	1.8628	1.7803	0.8961
HAZ	1.6591	1.5825	0.8180
T_{max}	19.3963	19.3937	0.9186

The errors remain moderate compared with the spread of each response. Tmax has the largest RMSE (19.4 °C) but also the highest R^2 (0.919). These two results are compatible: RMSE is

expressed in the units of the response, and Tmax varies over a much wider range than hardness or σ_U, whereas R^2 measures the fraction of the variation explained by the model, about 92% for Tmax. The HAZ model has the lowest R^2 (0.818) despite a small RMSE, which agrees with the larger scatter already noted for this response in Figure 5. The nearly equal RMSE and MAE values, particularly for Tmax, indicate that the validation errors were of similar size for all tests rather than dominated by a single outlier.

5. Conclusion

This study examined the effects of rotational speed (N), feed rate (S), and tool tilt angle (θ) on the ultimate tensile strength (σ_U), the maximum temperature recorded 10 mm from the weld centerline (Tmax), and the NZ and HAZ hardness of friction stir welded AA3003 joints, using a three-level full factorial design and RSM.

Within the tested ranges, the tilt angle had the largest effect on Tmax, and the rotational speed had the largest effect on NZ hardness and σ_U. Increasing N or θ raised Tmax and lowered the hardness of both the NZ and the HAZ, which indicates that the softening of these zones is controlled mainly by heat input. In contrast, σ_U increased with rotational speed and was lowest near the intermediate feed rate of 300 mm/min, so the conditions that favor strength differ from those that favor hardness. The clear interactions between the parameters, particularly between S and θ, show that they must be selected together rather than one at a time.

The regression models fitted the experimental data with R^2 values between 0.90 and 0.96 and predicted eight independent validation tests with R^2 values between 0.818 and 0.919, although they tended to underestimate the measured values. Multi-response optimization gave N = 1000 rpm, S = 400 mm/min, and θ = 0.5°, with predicted values of 122.7 MPa for σ_U, 49.2 HV in the NZ, 43.8 HV in the HAZ, and 196 °C for Tmax. This setting coincides with a tested run but lies at the limits of the investigated ranges.

The microstructural mechanisms proposed in this work were inferred from hardness and temperature data and should be verified by grain size measurements, macrographs, and fractography. Future work should also extend the parameter ranges around the predicted optimum and test whether data-driven models, such as artificial neural networks, describe the nonlinear interactions more accurately than the polynomial models used here.

6. Statements & Declarations

This research did not receive any specific grant from funding agencies in the public, commercial, or not-for-profit sectors.

Funding

The authors declare that no funds, grants, or other support were received during the preparation of this manuscript.

Competing Interests

The authors have no relevant financial or non-financial interests to disclose

Author Contributions

All authors contributed to the study conception and design. All authors read and approved the final manuscript.

Data availability Not applicable.

7. References

[1] W. M. Thomas, E. D. Nicholas, J. C. Needham, M. G. Murch, P. Temple-Smith, and C. J. Dawes, "Improvements relating to friction welding," International Patent Application WO1993010935A1, priority date 6 Dec. 1991, published 10 Jun. 1993.

[2] S. Kilic, F. Ozturk, and M. F. Demirdogen, "A comprehensive literature review on friction stir welding: Process parameters, joint integrity, and mechanical properties," *Journal of Engineering Research*, vol. 13, no. 1, pp. 122–130, Mar. 2025, doi: 10.1016/J.JER.2023.09.005.

[3] D. Texier *et al.*, "Fatigue performances of FSW and GMAW aluminum alloys welded joints: Competition between microstructural and structural-contact-fretting crack initiation," *Int. J. Fatigue*, vol. 116, pp. 220–233, Nov. 2018, doi: 10.1016/J.IJFATIGUE.2018.06.020.

[4] R. Al-Sabur and M. Serier, "Material Sustainability During Friction Stir Joining," in *Sustainable Machining and Green Manufacturing*, John Wiley & Sons, Ltd, 2024, ch. 7, pp. 131–153. doi: https://doi.org/10.1002/9781394197866.ch7.

[5] V. M. Magalhães, C. Leitão, and D. M. Rodrigues, "Friction stir welding industrialisation and research status," *Science and Technology of Welding and Joining*, vol. 23, no. 5, pp. 400–409, 2018, doi: 10.1080/13621718.2017.1403110.

[6] J. Jamal, B. Darras, and H. Kishawy, “A study on sustainability assessment of welding processes,” *Proc. Inst. Mech. Eng. B J. Eng. Manuf.*, vol. 234, no. 3, pp. 501–512, 2020, doi: 10.1177/0954405419875355.

[7] K. Fuse and V. Badheka, “Bobbin tool friction stir welding: a review,” *Science and Technology of Welding and Joining*, vol. 24, no. 4, pp. 277–304, 2019, doi: 10.1080/13621718.2018.1553655.

[8] H. Shirazi, S. Kheirandish, and H. Pouraliakbar, “Employing hooking and effective sheet thickness to achieve optimum failure load in lap joints of friction stir welded AA5456 aluminum,” *Theoretical and Applied Fracture Mechanics*, vol. 105, p. 102423, Feb. 2020, doi: 10.1016/J.TAFMEC.2019.102423.

[9] W. F. Xu, X. K. Wu, J. Ma, H. J. Lu, and Y. X. Luo, “Abnormal fracture of 7085 high strength aluminum alloy thick plate joint via friction stir welding,” *Journal of Materials Research and Technology*, vol. 8, no. 6, pp. 6029–6040, Nov. 2019, doi: 10.1016/J.JMRT.2019.09.077.

[10] B. Eren, M. A. Guvenc, and S. Mistikoglu, “Artificial Intelligence Applications for Friction Stir Welding: A Review,” *Metals and Materials International*, vol. 27, no. 2, pp. 193–219, 2021, doi: 10.1007/s12540-020-00854-y.

[11] C. Rajendran, K. Srinivasan, V. Balasubramanian, H. Balaji, and P. Selvaraj, “Identifying Combination of Friction Stir Welding Parameters to Maximize Strength of Lap Joints of AA2014-T6 Aluminum Alloy,” *Archives of Mechanical Technology and Materials*, vol. 37, no. 1, pp. 6–21, Jan. 2017, doi: 10.1515/amtm-2017-0002.

[12] H. J. Liu, H. Fujii, M. Maeda, and K. Nogi, “Tensile properties and fracture locations of friction-stir-welded joints of 2017-T351 aluminum alloy,” *J. Mater. Process. Technol.*, vol. 142, no. 3, pp. 692–696, Dec. 2003, doi: 10.1016/S0924-0136(03)00806-9.

[13] Y. Bozkurt and S. Duman, “The effect of welding parameters on the mechanical and microstructural properties of friction stir welded dissimilar AA 3003-H24 and 2124/SiC/25p-T4 alloy joints,” *Scientific Research and Essays*, vol. 6, no. 17, pp. 3702–3716, 2011, doi: 10.5897/SRE11.616.

[14] H. W. Huang and B. L. Ou, “Evolution of precipitation during different homogenization treatments in a 3003 aluminum alloy,” *Mater. Des.*, vol. 30, no. 7, pp. 2685–2692, Aug. 2009, doi: 10.1016/J.MATDES.2008.10.012.

[15] I. Chekalil, A. Miloudi, M. P. Planche, and A. Ghazi, “Prediction of mechanical behavior of friction stir welded joints of AA3003 aluminum alloy,” *Frattura ed Integrita Strutturale*, vol. 14, no. 54, pp. 153–168, Oct. 2020, doi: 10.3221/IGF-ESIS.54.11.

[16] S. Ugender, “Influence of tool pin profile and rotational speed on the formation of friction stir welding zone in AZ31 magnesium alloy,” *Journal of Magnesium and Alloys*, vol. 6, no. 2, pp. 205–213, Jun. 2018, doi: 10.1016/J.JMA.2018.05.001.

[17] Ø. Frigaard, Ø. Grong, and O. T. Midling, “A Process Model for Friction Stir Welding of Age Hardening Aluminum Alloys,” *Metallurgical and Materials Transactions A*, vol. 32, pp. 1189–1200, May 2001, doi: 10.1007/s11661-001-0128-4.

[18] A. Goyal, P. Kumar Rohilla, and A. Kumar Kaushik, “Optimization of Friction Stir Welding Parameters for AA3003 Aluminum Alloy Joints Using Response Surface Methodology,” *International Journal of Mechanics and Solids*, vol. 12, no. 1, pp. 15–26, 2017.

[19] A. Heidarzadeh, “Tensile behavior, microstructure, and substructure of the friction stir welded 70/30 brass joints: RSM, EBSD, and TEM study,” *Archives of Civil and Mechanical Engineering*, vol. 19, no. 1, pp. 137–146, Mar. 2019, doi: 10.1016/J.ACME.2018.09.009.

[20] A. Nait Salah, H. Mehdi, A. Mehmood, A. Wahab Hashmi, C. Malla, and R. Kumar, “Optimization of process parameters of friction stir welded joints of dissimilar aluminum alloys AA3003 and AA6061 by RSM,” *Mater. Today Proc.*, vol. 56, pp. 1675–1683, Jan. 2022, doi: 10.1016/J.MATPR.2021.10.288.

[21] G. Elatharasan and V. S. S. Kumar, “An Experimental Analysis and Optimization of Process Parameter on Friction Stir Welding of AA 6061-T6 Aluminum Alloy using RSM,” *Procedia Eng.*, vol. 64, pp. 1227–1234, Jan. 2013, doi: 10.1016/J.PROENG.2013.09.202.

[22] M. A. Ben Messaoud *et al.*, “Prediction and optimization of mechanical properties in FSWed AA6082-T6 joints using RSM and artificial neural networks,” *International Journal of Advanced Manufacturing Technology*, vol. 142, pp. 1931–1949, Jan. 2026, doi: 10.1007/s00170-025-17240-w.

[23] N. Dellal, M. Merzoug, A. Mimmi, A. Ghazi, and A. Lousdad, “EXPERIMENTAL BASED DETERMINATION AND ANALYSIS OF MECHANICAL PROPERTIES OF AA 3003 ALLOY WELDED WITH FRICTION STIR LAP WELDING PROCESS,” *Journal of Applied Engineering Science*, vol. 21, no. 2, pp. 451–461, 2023, doi: 10.5937/jaes0-40245.

[24] B. Abnar, M. Kazeminezhad, and A. H. Kokabi, “Effects of heat input in friction stir welding on microstructure and mechanical properties of AA3003-H18 plates,”

Transactions of Nonferrous Metals Society of China (English Edition), vol. 25, no. 7, pp. 2147–2155, Jul. 2015, doi: 10.1016/S1003-6326(15)63826-2.

[25] Y. B. Tan *et al.*, "A study on microstructure and mechanical properties of AA 3003 aluminum alloy joints by underwater friction stir welding," *Mater. Charact.*, vol. 127, pp. 41–52, May 2017, doi: 10.1016/J.MATCHAR.2017.01.039.

[26] M. A. Abdulrehman, S. H. Challoob, and I. I. Marhoon, "Investigation of mechanical and numerical properties of friction stir welding (FSW) for 3003 - H14 aluminum alloys," in *Defect and Diffusion Forum*, Trans Tech Publications Ltd, 2020, pp. 106–116. doi: 10.4028/www.scientific.net/DDF.398.106.

[27] M. Dehghani, S. A. A. A. Mousavi, and A. Amadeh, "Effects of welding parameters and tool geometry on properties of 3003-H18 aluminum alloy to mild steel friction stir weld," *Transactions of Nonferrous Metals Society of China*, vol. 23, no. 7, pp. 1957–1965, Jul. 2013, doi: 10.1016/S1003-6326(13)62683-7.

[28] M. Maeda, H. Liu, H. Fujii, and T. Shibayanagi, "Temperature Field in the Vicinity of FSW-Tool During Friction Stir Welding of Aluminium Alloys," *Welding in the World*, vol. 49, no. 3, pp. 69–75, 2005, doi: 10.1007/BF03266478.

[29] D. G. Andrade, C. Leitão, N. Dialami, M. Chiumenti, and D. M. Rodrigues, "Analysis of contact conditions and its influence on strain rate and temperature in friction stir welding," *Int. J. Mech. Sci.*, vol. 191, p. 106095, Feb. 2021, doi: 10.1016/J.IJMECSCI.2020.106095.

[30] Y. M. Hwang, Z. W. Kang, Y. C. Chiou, and H. H. Hsu, "Experimental study on temperature distributions within the workpiece during friction stir welding of aluminum alloys," *Int. J. Mach. Tools Manuf.*, vol. 48, no. 7–8, pp. 778–787, Jun. 2008, doi: 10.1016/J.IJMACHTOOLS.2007.12.003.

[31] A. Belaribi, I. Chekalil, A. Miloudi, M. A. Ben Messaoud, and A. Zoukel, "Effect of welding parameters and response surface method based on prediction of maximum temperature generated during friction stir welding of AA3003," *Materials Physics and Mechanics*, vol. 53, no. 6, pp. 201–212, 2025, doi: 10.18149/MPM.5362025_15.

[32] Stat-Ease Inc., "Design-Expert, Version 13," Minneapolis, MN, USA.

[33] A. Mishra, A. Miloudi, E. M. Sefene, C. Arroussi, I. Chekalil, and B. G. N. Muthanna, "Hybrid deep learning model to predict the ultimate tensile strength of friction stir welded joints," *Eng. Appl. Artif. Intell.*, vol. 154, p. 111001, Aug. 2025, doi: 10.1016/J.ENGAPPAI.2025.111001.

[34] I. Sabry, V. P. Singh, M. Alkhedher, N. E. El-Zathry, A. H. I. Mourad, and M. Naseri, "Effect of rotational speed and penetration depth on Al-Mg-Si welded T-joints through underwater and conventional friction stir welding," *Journal of Advanced Joining Processes*, vol. 9, p. 100207, Jun. 2024, doi: 10.1016/J.JAJP.2024.100207.

[35] F. Zhang, X. Su, Z. Chen, and Z. Nie, "Effect of welding parameters on microstructure and mechanical properties of friction stir welded joints of a super high strength Al-Zn-Mg-Cu aluminum alloy," *Mater. Des.*, vol. 67, pp. 483–491, Feb. 2015, doi: 10.1016/j.matdes.2014.10.055.

[36] A. M. Takhakh and A. M. Abdullah, "The Optimization Conditions of Friction Stir Welding (FSW) for Different Rotational and Weld speeds," *Nahrain University College of Engineering Journal*, vol. 15, no. 2, pp. 187–196, Sep. 2012, [Online]. Available: https://oldjournal.eng.nahrainuniv.edu.iq/index.php/main/article/view/623

[37] C. Rajendran, K. Srinivasan, V. Balasubramanian, H. Balaji, and P. Selvaraj, "EFFECT OF TOOL TILT ANGLE ON MICROSTRUCTURAL CHARACTERISTICS OF FRICTION STIR WELDED LAP JOINTS OF AA2014-T6 ALUMINUM ALLOY JOINTS," *Journal of Manufacturing Engineering*, vol. 12, no. 3, pp. 120–126, 2017, [Online]. Available: www.smenec.org

[38] S. D. Meshram and G. Madhusudhan Reddy, "Influence of tool tilt angle on material flow and defect generation in friction stir welding of AA2219," *Def. Sci. J.*, vol. 68, no. 5, pp. 512–518, Sep. 2018, doi: 10.14429/dsj.68.12027.

[39] H. Aghajani Derazkola, N. Kordani, and H. Aghajani Derazkola, "Effects of friction stir welding tool tilt angle on properties of Al-Mg-Si alloy T-joint," *CIRP J. Manuf. Sci. Technol.*, vol. 33, pp. 264–276, May 2021, doi: 10.1016/j.cirpj.2021.03.015.

[40] S. Kumar, J. K. Katiyar, and B. S. Roy, "Influence of tool tilt angle on physical, thermal, and mechanical properties of friction stir welded Al-Cu-Li alloys," *Mater. Today Commun.*, vol. 34, Art. no. 105348, Mar. 2023, doi: 10.1016/j.mtcomm.2023.105348.

[41] M. Tutar, H. Aydin, C. Yuce, N. Yavuz, and A. Bayram, "The optimisation of process parameters for friction stir spot-welded AA3003-H12 aluminium alloy using a Taguchi orthogonal array," *Mater. Des.*, vol. 63, pp. 789–797, Nov. 2014, doi: 10.1016/J.MATDES.2014.07.003.

[42] M. M. El Rayes, M. S. Soliman, A. T. Abbas, D. Y. Pimenov, I. N. Erdakov, and M. M. Abdel-Mawla, "Effect of Feed Rate in FSW on the Mechanical and Microstructural Properties of AA5754 Joints," *Advances in Materials Science and Engineering*, vol. 2019, Art. no. 4156176, 2019, doi: 10.1155/2019/4156176.

[43] S. Delijaicov, P. A. de Oliveira Silva, H. B. Resende, and M. H. F. Batalha, “Effect of weld parameters on residual stress, hardness and microstructure of dissimilar AA2024-T3 and AA7475-T761 friction stir welded joints,” *Materials Research*, vol. 21, no. 6, Art. no. e20180108, 2018, doi: 10.1590/1980-5373-mr-2018-0108.

[44] H. T. Elmetwally, H. N. SaadAllah, M. S. Abd-Elhady, R. K. Abdel-Magied, and A. A. Abd-Eltwab, “Examination of the parameters effect on Al-Cu FSW welded butt joints using formability consent,” *Babylonian Journal of Mechanical Engineering*, vol. 2024, pp. 34–48, 2024, doi: 10.58496/BJME/2024/006.

[45] M. Pourali, A. Abdollah-zadeh, T. Saeid, and F. Kargar, “Influence of welding parameters on intermetallic compounds formation in dissimilar steel/aluminum friction stir welds,” *J. Alloys Compd.*, vol. 715, pp. 1–8, Aug. 2017, doi: 10.1016/j.jallcom.2017.04.272.

[46] A. Laska, B. Sadeghi, B. Sadeghian, A. Taherizadeh, M. Szkodo, and P. Cavaliere, “Temperature Evolution, Material Flow, and Resulting Mechanical Properties as a Function of Tool Geometry during Friction Stir Welding of AA6082,” *J. Mater. Eng. Perform.*, vol. 32, no. 23, pp. 10655–10668, Dec. 2023, doi: 10.1007/s11665-023-08671-1.

[47] I. Chekalil *et al.*, “Effect of corrosion environments on the mechanical properties of friction stir welded aluminum alloy AA3003,” *Journal of Materials Research and Technology*, vol. 33, pp. 2353–2364, Nov. 2024, doi: 10.1016/j.jmrt.2024.09.167.

[48] R. Sivasankara Raju, Jagadish, C. J. Rao, S. Kumar Aadapa, and S. Yanda, “Predication of temperature distribution and strain during FSW of dissimilar Aluminum alloys using Deform 3D,” *Mater. Today Proc.*, vol. 59, pp. 1760–1767, Jan. 2022, doi: 10.1016/J.MATPR.2022.04.371.

[49] A. Belaribi *et al.*, “Effect of welding parameters and artificial intelligence-based prediction of maximum temperature in friction stir welding of AA3003 alloy,” *International Journal of Advanced Manufacturing Technology*, vol. 141, no. 7–8, pp. 3681–3693, Dec. 2025, doi: 10.1007/s00170-025-16847-3.